Control of a Tetherless Miniature Robot using Static Magnetic Fields

Abraham G.J. Harbers* and Islam S.M. Khalil

University of Twente, Faculty of Engineering Technology,
Drienerlolaan 5, 7522 NB, Enschede, The Netherlands
**corresponding author a.g.j.harbers@student.utwente.nl*

ABSTRACT: Capsule endoscopy is used to examine hard-to-access regions of the digestive system which flexible endoscopes cannot reach. The capsule with a built-in camera system is ingested and the images are wirelessly transmitted to a receiver, after which they can be studied by an operator. Some of the issues involved in capsule endoscopy include capsule retention and the failure to examine the full small bowel. This paper explores the possibilities of adding wireless control using static magnetic fields to capsule endoscopy. The implementation of an electromagnetic tri-axial Helmholtz coil system in a capsule allows for a controlled dipole moment to be generated. This moment, coupled with an external static field, is used to generate magnetic torque around the robot's axes. Controllability of the miniature robot is demonstrated under a state feedback control system and controlled directional control is demonstrated in a three-dimensional space. Furthermore, control of continuous rotation is demonstrated using a path-mapped reference input, allowing for positional control using helical propulsion.

Key words: control, controllability, magnetic control, stability, static field, tri-axial coils

1 INTRODUCTION

Since the 1800s, flexible endoscopes are used to navigate the natural pathways within the human body without having to expose the area itself. Flexible endoscopes allow for imagery within the body, primarily in the stomach and colon areas. In the 1990s, new developments by Iddan *et al.* [1] in the field of minimally invasive surgery have resulted in capsule endoscopy, which makes use of microrobots designed to improve on the flexible scopes. First developed in 2001, the robots are small, wireless, tetherless, pill-shaped capsules which can be ingested to perform the endoscopic functions of a flexible instrument [2]. The major advantage of tetherless miniature robots over traditional scopes is that the capsules are completely wireless, allowing for a less invasive way of navigating the natural pathways of the human body. Furthermore, they have the ability to reach locations inaccessible to tethered flexible endoscopes [3, 4]. The images or videos are recorded, wirelessly transmitted, and received by the clinicians, making it an easier and faster experience for both the patient and the clinicians, compared to a flexible endoscope.

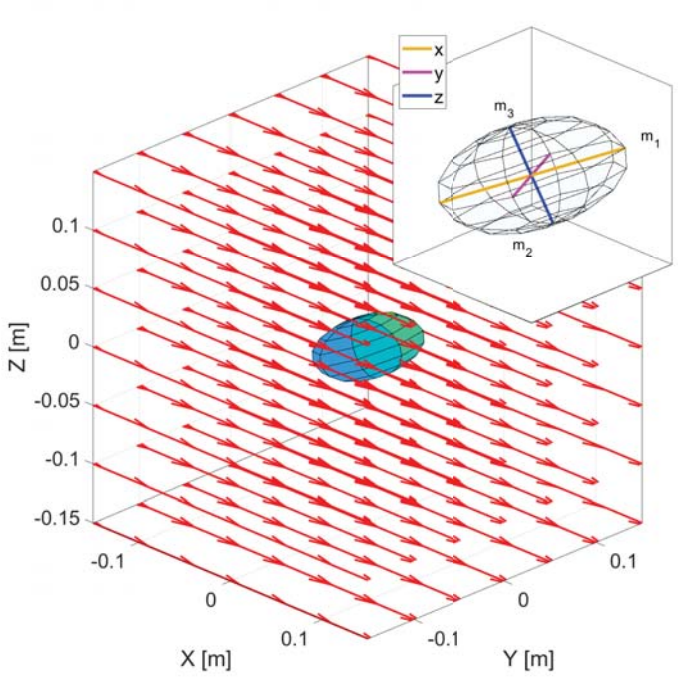

Fig. 1: Directional control of a miniaturized capsule is achieved in a uniform magnetic field. The capsule is integrated with a tri-axial electromagnetic coil system to control its magnetic dipole moment (m_1, m_2, m_3). The axis x, y and z represent the local material frame of reference $\mathfrak{R}_c$, while X, Y and Z represent the global frame $\mathfrak{R}_0$.

Some of the complications of capsule endoscopy include capsule retention inside the body, which can result in small bowel obstruction and lead to surgery [5, 6]. In addition, capsule retention can result

in capsule perforation [7, 8], although it is a rare occurrence. Furthermore, the failure to examine the full small bowel is estimated to be 20% [9], in which case the procedure must be repeated. This happens mainly because of the slow movement of the capsule through the digestive system and its limited battery life, resulting in a loss of power before reaching the desired area. By adding control to a capsule, the procedure can become faster and more accurate than can be obtained by natural bowel movements alone. The medical professionals would be able to control the robot to a desired orientation and position, thereby allowing for control of what is examined during the procedure. Magnetic control can provide the wireless control without the need for an on-board actuator or moving parts, resulting in the ability for a simple and reliable design.

One method to control the motion of the robot is achieved by dynamic magnetic fields. There are multiple systems and methods to control a magnetic field to actuate a small object. One possibility is to have a position and current-controlled electromagnetic system. In a study by Yesin *et al.* [10], a system with two rigidly connected pairs of electromagnets create two superimposed fields, allowing one uniform field to be manipulated by another by the means of superposition. Using position control, a microrobot can be manipulated. A different system was designed by Grady *et al.* [11] in which a small permanent magnet was controlled within a canine brain. It utilizes a single position-controlled coil to control the magnet.

An alternative method to control the robot depends on stationary, current-controlled magnets. The OctoMag system [12], for example, uses eight electromagnets in a focused ring to manipulate a microrobot. It focuses on eye surgery and allows the microrobot to be positioned within the retina.

Magnetic torque is generated by an interaction between a dipole moment, provided by a permanent magnet [13], and a magnetic field, provided by large coils in the surrounding area. This paper presents an alternative approach, where the control system is embedded within the robot itself. By implementing a system of orthogonal electromagnetic tri-axial Helmholtz coils [14], the robot can generate a dipole moment in any direction. Together with an embedded control system, the robot should be able to rotate in a static magnetic field. One of the possible applications can be the use within Magnetic Resonance Imaging (MRI) systems [15], which are already widely available in hospitals. However, since magnetic control can result in limitations, the research question becomes: Is it possible to achieve directional control in a unidirectional static magnet field using a controlled moment? The answer is investigated by modelling the rotational dynamics of the robot in low Reynolds numbers and investigating state feedback control.

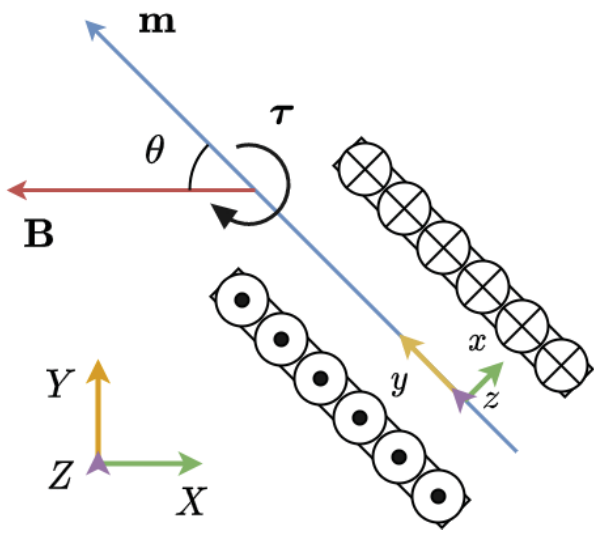

Fig. 2: Schematic representation of the magnetic torque τ generated by an interaction between the dipole moment $\mathbf{m}$ and an external field $\mathbf{B}$. The dipole moment $\mathbf{m}$ is generated by a current flowing through a solenoid.

2 METHOD AND RESULTS

Until now, little research has gone into implementing a control system into a capsule and using static magnetic fields to control the system. To test the controllability of the robot, a kinematic model was created. In this section, the dynamic model and control systems are presented.

2.1 Governing Equations

A tri-axial coil consists of 3 perpendicular solenoids, which act as 3 dipoles that can be either turned off or on with a controlled magnitude. The solenoids generate a magnetic dipole moment $\mathbf{m} \in \mathbb{R}^{3\times1}$, which interacts with the external magnetic field $\mathbf{B} \in \mathbb{R}^{3\times1}$ to generate a magnetic torque, as is shown in Fig. 2. The generated magnetic torque is determined by

$$\boldsymbol{\tau_m} = \mathbf{m} \times \mathbf{B}, \tag{1}$$

where $\boldsymbol{\tau_m} \in \mathbb{R}^{3\times1}$ is the magnetic torque exerted on the net magnetic moment of the tri-axial coils. The torque generated gives a rotation around the axis of a tri-axial coil, therefore the robot orients itself to a different direction. The magnetic dipole moment of a solenoid is given by

$$m_i = NI_iS, \tag{2}$$

where I is the current flowing through the coil, N is the number of turns and S is the vector area. When equation (2) is substituted into equation (1), the current flowing through the coils is related to the torque by

$$\boldsymbol{\tau_m} = \begin{bmatrix} NSI_1 \\ NSI_2 \\ NSI_3 \end{bmatrix} \times \begin{bmatrix} B_1 \\ B_2 \\ B_3 \end{bmatrix}. \tag{3}$$

The Reynolds number, the ratio between the viscous and inertia properties of a fluid, is determined by

$$Re = \frac{\rho u D}{\mu} << 10, \tag{4}$$

where ρ is the density, u is the relative velocity to the flow, D is the characteristic length of the capsule and μ is the dynamic viscosity. Because of the high viscous properties present in most body fluids and the small size of the robot, the Reynolds number is assumed to be very small. This assumption allows for the application of Stokes' law, expressed as

$$F_d = 6\pi\eta r U, \tag{5}$$

where F_d is the drag force, η is the viscosity of the medium, r is the radius of the object and U is the velocity of the object relative to the fluid. However, to transform Stokes' Law from a spherical to an ellipsoidal application, the equation must be modified. Discussed in a paper by Bayly *et al.* [16], the drag force and torque for an ellipsoid are given by

$$\begin{aligned} F_{d,x} &= 6a\pi\eta C_1 U_x, \\ F_{d,y} &= 6a\pi\eta C_2 U_y, \\ \boldsymbol{\tau_d} &= 8ab^2\pi\eta C_3 \boldsymbol{\omega}, \end{aligned} \tag{6}$$

where a is the major diameter of the ellipsoid and b is the minor diameter of the ellipsoid. The coefficients C_1, C_2 and C_3 are given by

$$\begin{aligned} C_1 &= \frac{8}{3}e^3\Big[-2e + (1+e^2)\ln\frac{1+e}{1-e}\Big]^{-1}, \\ C_2 &= \frac{16}{3}e^3\Big[2e + (3e^2-1)\ln\frac{1+e}{1-e}\Big]^{-1}, \\ C_3 &= \frac{4}{3}e^3\Big(\frac{e-e^2}{1+e^2}\Big)\Big[-2e + (1+e^2)\ln\frac{1+e}{1-e}\Big]^{-1}, \end{aligned} \tag{7}$$

where $e = \sqrt{1 - b^2/a^2}$. It is assumed that the gravity is balanced out by the buoyant forces on the capsule [13] and the velocity of the stream is negligible. Therefore the drag torque and magnetic torque are the only moments acting on the capsule [17], which means that the torques result in an equation given by

$$\boldsymbol{\tau_d} = \boldsymbol{\tau_m}, \tag{8}$$

substituting equation (1) and (6) into equation (8) yields

$$\begin{aligned} \boldsymbol{\omega} &= \frac{\boldsymbol{\tau_m}}{8ab^2\pi\eta C_3} \\ &= \frac{\mathbf{m} \times \mathbf{B}}{8ab^2\pi\eta C_3}, \end{aligned} \tag{9}$$

Using equation (9), the dipole moment is related to the angular velocity, which can be integrated to a difference in rotational angles. The controller is used to determine the optimal current of each coil.

2.2 Magnetic Field Parameters

The magnetic field $\mathbf{B}$ can be described by the coils producing it and the current that flows through them. Using multiple electromagnets, also present in the OctoMag system [12], various degrees of complex magnetic fields can be generated. The overall equation for a magnetic field generated by an n number of coils is defined as

$$\mathbf{B} = \mathcal{B}\mathbf{I_{ex}}, \tag{10}$$

where $\mathcal{B} \in \mathbb{R}^{3\times n}$ is the magnetic field current-mapping and $\mathbf{I_{ex}} \in \mathbb{R}^{n\times1}$ is the current flowing through the external coils. To increase the overall applicability of the system, the magnetic field is

chosen to be uniform at every position. This can be generated by several magnetic systems [18], thus increasing the chances of the concept being compatible with as many systems as possible.

2.3 Kinematics of the Miniature Robot

To achieve directional control of the robot, the robot should be able to rotate accordingly. In this section, the three-dimensional rotational kinematics of a microrobot suspended in a medium are presented. First, a distinction is made between two reference frames; the global fixed frame $\mathfrak{R}_0$ and the dynamic local frame of the capsule $\mathfrak{R}_c$. The local frame is placed parallel to the tri-axial coil, and its movement coincides with the axes. To express the local frame $\mathfrak{R}_c$ in $\mathfrak{R}_0$, Tait-Bryan angles are utilized. Tait-Bryan angles represent rotational angles around the three axes similar to Euler angles; ϕ is around the x-axis, θ is around the y-axis and ψ is around the z-axis [19]. In order to transform local coordinates to global coordinates, rotation matrices are used, defined by

$$\begin{aligned}
\mathbf{R_X} &= \begin{bmatrix} 1 & 0 & 0 \\ 0 & \cos\phi & -\sin\phi \\ 0 & \sin\phi & \cos\phi \end{bmatrix} \\
\mathbf{R_Y} &= \begin{bmatrix} \cos\theta & 0 & \sin\theta \\ 0 & 1 & 0 \\ -\sin\theta & 0 & \cos\theta \end{bmatrix} \\
\mathbf{R_Z} &= \begin{bmatrix} \cos\psi & -\sin\psi & 0 \\ \sin\psi & \cos\psi & 0 \\ 0 & 0 & 1 \end{bmatrix},
\end{aligned} \tag{11}$$

where ϕ, ψ and θ are the angles around the axes, grouped as $\mathbf{\Theta} \in \mathbb{R}^{3\times1}$. Since matrix multiplication is non-commutative, the order of matrix operations influences the outcomes of the operations. In this research, the 3-2-1 Euler intrinsic angles, also called the z-y'-x'' intrinsic rotations are used because of its use in the aircraft industry where it is known as yaw, pitch and roll. The intrinsic properties of these operations mean the rotations will occur around dynamic axes of the capsule, which are adjusted after each rotation, in the z-y-x order. An alternative method is the use of the x-y-z extrinsic angles. The order remains is identical to the 3-2-1 Euler intrinsic angles, but instead of rotating around the object axes, it rotates around the fixed frame axes of $\mathfrak{R}_0$. Both rotational operations are displayed in equation (12) and (13) and deliver different results. (The angle $-\theta$ is used because the default angle is pointed in the $-z$ direction.) The transposed version of the rotation matrix can be used to transform coordinates or vectors from the global frame $\mathfrak{R}_0$ to the local frame $\mathfrak{R}_c$.

$$\begin{bmatrix} x_{in} \\ y_{in} \\ z_{in} \end{bmatrix} = \mathbf{R_Z}(\psi)\mathbf{R_Y}(-\theta)\mathbf{R_X}(\phi) \begin{bmatrix} X \\ Y \\ Z \end{bmatrix}, \tag{12}$$

$$\begin{bmatrix} x_{ex} \\ y_{ex} \\ z_{ex} \end{bmatrix} = \mathbf{R_X}(\phi)\mathbf{R_Y}(-\theta)\mathbf{R_Z}(\psi) \begin{bmatrix} X \\ Y \\ Z \end{bmatrix}. \tag{13}$$

Ultimately, the 3-2-1 Euler intrinsic angles were utilized to achieve better control of the rolling motion of the robot, which is utilized in generating propulsion. Therefore, equation (12) is utilized to determine the rotations of the robot in the kinematic model.

2.4 Controllability of the Miniature Robot

The control of the microrobot is integral to the concept since its ability to generate a suitable dipole moment is the driving force behind the robot. One of the crucial parts of designing the controller is the controllability of the robot. The controllability of a system dictates whether the inputs of a system are able to reach the states.

The use of magnetic control paired with a unidirectional static magnetic field comes with restrictions due to the nature of the generated torques and forces. One restriction of the magnetic torque is the alignment of coils with the direction of the external magnetic field. For instance, assuming $\mathbf{B}$ is a uniform field in the x-direction and coil 1 of the tri-axial system is aligned with $\mathbf{B}$, the equation for the torque becomes

$$\boldsymbol{\tau_m} = \mathbf{m} \times \mathbf{B} = \begin{bmatrix} m_1 \\ m_2 \\ m_3 \end{bmatrix} \times \begin{bmatrix} B_x \\ 0 \\ 0 \end{bmatrix} = \begin{bmatrix} 0 \\ \tau_2 \\ \tau_3 \end{bmatrix}. \tag{14}$$

No combination of dipole moments can generate a torque around the aligned axis, limiting the orientational movement of the robot.

A rank analysis is a tool to check system controllability. To do that, a simple proportional controller is used. An alternative method to write

equation equation (1) is

$$\begin{aligned}\boldsymbol{\tau_m} &= -\mathbf{B} \times \mathbf{m} \\ &= [-\mathbf{B}]_\times \mathbf{m},\end{aligned} \tag{15}$$

where $[-\mathbf{B}]_\times \in \mathbb{R}^{3\times3}$ is the skew-symmetric matrix defined by

$$[-\mathbf{B}]_\times = \begin{bmatrix} 0 & -B_3 & B_2 \\ B_3 & 0 & -B_1 \\ -B_2 & B_1 & 0 \end{bmatrix}. \tag{16}$$

This representation allows us to write the system as a linear set of equations [20], which is given by

$$\begin{aligned}\boldsymbol{\tau_m} &= [-\mathbf{B}]_\times \mathbf{m} = \mathbf{K_p e} \\ &= \begin{bmatrix} 0 & -B_3 & B_2 \\ B_3 & 0 & -B_1 \\ -B_2 & B_1 & 0 \end{bmatrix} \begin{bmatrix} m_1 \\ m_2 \\ m_3 \end{bmatrix} = \begin{bmatrix} K_{p,1}e_1 \\ K_{p,2}e_2 \\ K_{p,3}e_3 \end{bmatrix},\end{aligned} \tag{17}$$

where $\mathbf{K_p} \in \mathbb{R}^{3\times3}$ is the proportional gain matrix and $\mathbf{e} \in \mathbb{R}^{3\times1}$ is the angular error defined by

$$\mathbf{e} = \boldsymbol{\Theta}_{des} - \boldsymbol{\Theta}. \tag{18}$$

Because of the skew-symmetric properties of $[-\mathbf{B}]_\times$ [21], the rank of the system is 2, therefore one of the states cannot reach its desired value. As a consequence of this property, the system is unable to reach its desired position, and a different form of control is needed.

2.5 Regulation by Full State Feedback

In order to gain full controllability, coupling is needed between the different angles. One method of achieving this coupling is by introducing full state feedback, based on the state-space equations. The state-space representation is defined as

$$\begin{aligned}\dot{\mathbf{x}}(t) &= \mathbf{A}(t)\mathbf{x}(t) + \mathbf{B}(t)\mathbf{u}(t), \\ \mathbf{y}(t) &= \mathbf{C}(t)\mathbf{x}(t) + \mathbf{D}(t)\mathbf{u}(t),\end{aligned} \tag{19}$$

where $\mathbf{x}(t) \in \mathbb{R}^n$ is the state vector, $\mathbf{y}(t) \in \mathbb{R}^q$ is the output vector, $\mathbf{u}(t) \in \mathbb{R}^p$ is the input vector, $\mathbf{A}(t) \in \mathbb{R}^{n\times n}$ is the state matrix, $\mathbf{B}(t) \in \mathbb{R}^{n\times p}$ is the input matrix, $\mathbf{C}(t) \in \mathbb{R}^{q\times n}$ is the output matrix and $\mathbf{D}(t) \in \mathbb{R}^{q\times p}$ is the feedthrough matrix. To increase clarity in the equations, the constant of Stokes' Law is defined as

$$f \equiv 8ab^2\pi\eta C_3, \tag{20}$$

which means equation (8) can be written as

$$\begin{aligned} f\dot{\mathbf{x}} &= \mathbf{m} \times \mathbf{B}, \\ \dot{\mathbf{x}} &= \frac{1}{f}(\mathbf{m} \times \mathbf{B}),\end{aligned} \tag{21}$$

where $\mathbf{x} \in \mathbb{R}^{3\times1}$ is the state of the system, in this case described by

$$\mathbf{x} \equiv \boldsymbol{\Theta}, \tag{22}$$

where $\boldsymbol{\Theta} \in \mathbb{R}^{3\times1}$ is the angle vector. To utilize full state feedback, a state matrix $\mathbf{A}(t)$ is designed to generate coupling between the states, allowing for full controllability of the system. Furthermore, auxiliary control is needed for stability in the system. This can be utilized when equation (21) is set to full state feedback, given by

$$\begin{aligned}\frac{1}{f}(\mathbf{m} \times \mathbf{B}) &= \mathbf{A}(t)\mathbf{x}(t) + \mathbf{B}(t)\mathbf{u}(t) \\ &= \dot{\mathbf{x}},\end{aligned} \tag{23}$$

where $\mathbf{u}(t)$ is set to a proportional input by

$$\mathbf{u}(t) = -\mathbf{K}\mathbf{x}(t), \tag{24}$$

where $\mathbf{K} \in \mathbb{R}^{3\times3}$ is a proportional gain matrix. In order give $\mathbf{A}(t)$ the desired structure, the state gain vector is used, given by

$$\mathbf{K_A} \equiv \begin{bmatrix} K_{A,1} & K_{A,2} & K_{A,3} & K_{A,4} & K_{A,5} \end{bmatrix}, \tag{25}$$

where $\mathbf{K_A} \in \mathbb{R}^{1\times5}$ is the state gain vector. Full coupling between the states was achieved by setting $\mathbf{A}(t)$ as

$$\mathbf{A}(t) \equiv \begin{bmatrix} K_{A,4} & K_{A,3} & 0 \\ 0 & 0 & K_{A,2} \\ K_{A,5} & 0 & K_{A,1} \end{bmatrix}. \tag{26}$$

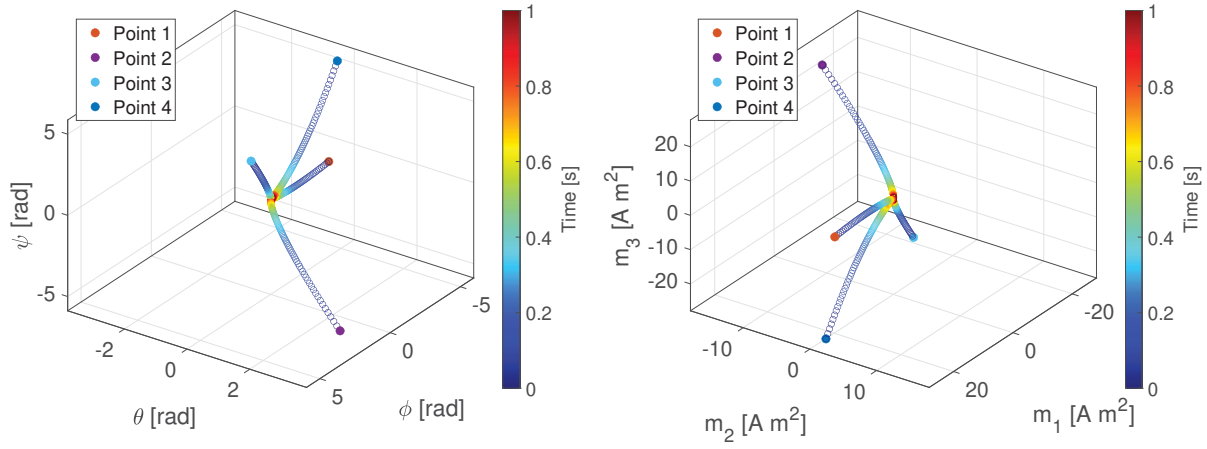

Fig. 3: Angular position and dipole moment of a simulated microrobot as a function of time powered by full state feedback. Each starting point is a randomly generated position, and the positions move to the origin, which is located at [0,0,0].

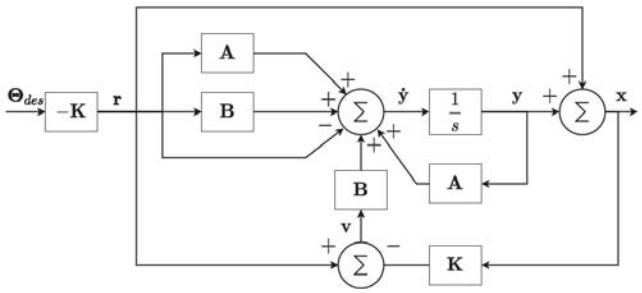

Fig. 4: Block diagram of the full state feedback controller.

Furthermore, an auxiliary control matrix is set to an arbitrary value β by

$$\mathbf{B}(t) \equiv \begin{bmatrix} \beta_1 & 0 & 0 \\ 0 & \beta_2 & 0 \\ 0 & 0 & \beta_3 \end{bmatrix}. \tag{27}$$

Using these matrices, equation (21) is rewritten into

$$\begin{aligned} \begin{bmatrix} \dot{x}_1 \\ \dot{x}_2 \\ \dot{x}_3 \end{bmatrix} &= \begin{bmatrix} K_{A,4} & K_{A,3} & 0 \\ 0 & 0 & K_{A,2} \\ K_{A,5} & 0 & K_{A,1} \end{bmatrix} \begin{bmatrix} x_1 \\ x_2 \\ x_3 \end{bmatrix} \\ &\quad - \begin{bmatrix} \beta_1 & 0 & 0 \\ 0 & \beta_2 & 0 \\ 0 & 0 & \beta_3 \end{bmatrix} \begin{bmatrix} K_1 & 0 & 0 \\ 0 & K_2 & 0 \\ 0 & 0 & K_3 \end{bmatrix} \begin{bmatrix} x_1 \\ x_2 \\ x_3 \end{bmatrix}, \end{aligned} \tag{28}$$

which can be written as

$$\dot{\mathbf{x}} = (\mathbf{A} - \mathbf{BK})\mathbf{x}. \tag{29}$$

This system is full rank, which means each of the states is fully controllable. To achieve stability, the inequality

$$\mathbf{A} - \mathbf{BK} < 0 \tag{30}$$

has to hold, after which the states will converge to the origin in a finite time. This is called a regulator. The regulation control action enables the states to converge regardless of the initial conditions. As long as equation (30) holds, the controller will return the system to its origin.

In Fig. 3 the results of several simulation tests based on random starting points are shown. The angles of the microrobot go the origin located at $\mathbf{\Theta} = [0, 0, 0]$. The values of the $\mathbf{K}$ matrix can be changed to reach the final state faster or slower, which allows for control over both speed and accuracy. Furthermore, the $\mathbf{B}$ matrix can be altered to include feed-forward, therefore increasing the possibilities for controller tuning to improve performance and stability. Feed-forward is however not further discussed in this paper. An important note is that mostly arbitrary values for $\mathbf{A}, \mathbf{B}$ and $\mathbf{K}$ are used. Therefore, the results do not represent feasible values for the inputs and outputs of the system.

2.6 Shifting the Origin

The state feedback controller allows for a regulation of the system. By shifting the origin to a desired position, the robot will rotate to that position, meaning full control of orientation is achieved. To do this, the entire system is to be shifted, and a shift vector $\mathbf{r} \in \mathbb{R}^{3\times1}$ is introduced, which functions as a reference. The shift vector is used to describe the shifted states by

$$\begin{aligned} \dot{\mathbf{y}}(t) &= \dot{\mathbf{x}}(t) - \mathbf{r}, \\ \mathbf{y}(t) &= \mathbf{x}(t) - \mathbf{r}, \end{aligned} \tag{31}$$

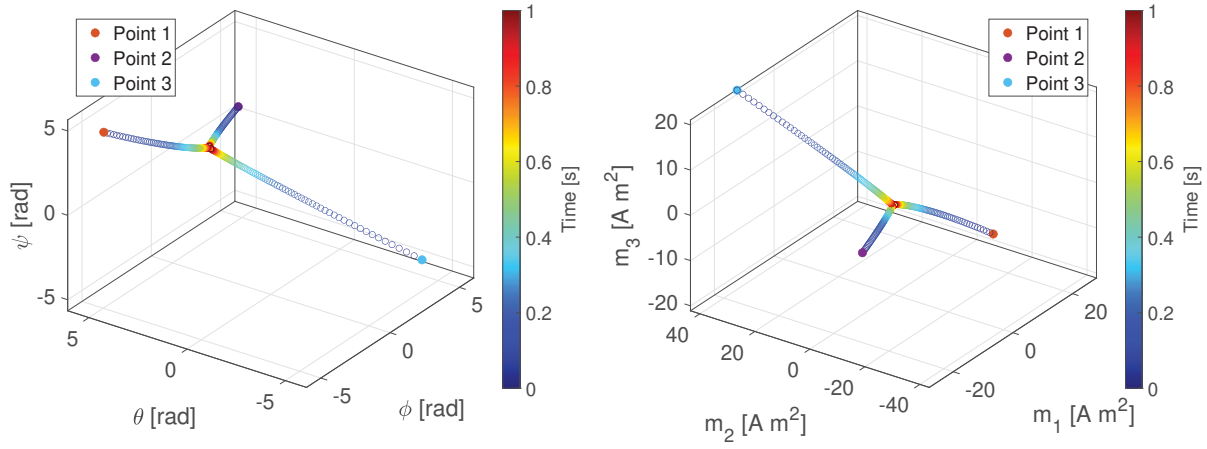

Fig. 5: Angular position and dipole moment of a simulated microrobot as a function of time powered by a shifted full state feedback. Each starting point is a randomly generated position, and the positions move to the origin, which is located at $[\text{-}0.5\pi, 2\pi, \pi]$.

where $\mathbf{y} \in \mathbb{R}^{3\times1}$ is the shifted state. Furthermore, the input of the system is shifted by $\mathbf{r}$, defined as

$$\mathbf{v}(t) = \mathbf{u}(t) - \mathbf{r}, \tag{32}$$

where $\mathbf{v}(t)$ is the shifted input. Because the input of the system remains the same, equation (24) still holds, which means that $\mathbf{v}$ can be described as

$$\begin{aligned}\mathbf{v}(t) &= -\mathbf{K}\mathbf{x}(t) - \mathbf{r} \\ &= -\mathbf{K}(\mathbf{y}(t) + \mathbf{r}) - \mathbf{r}.\end{aligned} \tag{33}$$

By using equation (21) and (31), the shifted state is determined by

$$\begin{aligned}\dot{\mathbf{y}}(t) &= [\mathbf{A}\mathbf{x}(t) + \mathbf{B}\mathbf{u}(t)] - \mathbf{r} \\ &= [\mathbf{A}(\mathbf{y}(t) + \mathbf{r}) + \mathbf{B}(\mathbf{v}(t) + \mathbf{r})] - \mathbf{r} \\ &= \mathbf{A}\mathbf{y}(t) + \mathbf{B}\mathbf{v}(t) + \mathbf{A}\mathbf{r} + \mathbf{B}\mathbf{r} - \mathbf{r}.\end{aligned} \tag{34}$$

By using the relations of equation (31), the original states can be determined and used to determine the states for $t = t + 1$. A block diagram of the shifted system is displayed in Fig. 4.
These equations allow the control system to manoeuvre the robot to a desired rotation, as is shown in Fig. 5. It reaches the shifted origin in a similar timeframe as the zero-origin, which means performance is not impacted. Furthermore, as is displayed in Fig. 6, the error, defined by equation (18), goes close to zero. As is shown in the figure, the angles converge at a very similar time, even though the initial errors are different from another.

An important note regarding the reference $\mathbf{r}$ is that it has to be modified by a counter-acting gain. In equation (34), the shifting properties of $\mathbf{r}$ are counteracted by a subtraction of $\mathbf{r}$. However, because $\mathbf{v}(t)$ is a function of $\mathbf{K}\mathbf{r}$, the combination is not removed. To combat this, the desired angles are multiplied by a counter-acting gain, which is done by

$$\mathbf{r} = \mathbf{K}\boldsymbol{\Theta}_{des}, \tag{35}$$

where $\boldsymbol{\Theta}_{des} \in \mathbb{R}^{3\times1}$ is the desired angle vector and $\mathbf{K} \in \mathbb{R}^{3\times3}$ is the proportional gain matrix. This equation ensures the desired position is reached, instead of a fraction of it.

2.7 Propulsion Using Rotation

Full orientational control is obtained using the shifted system of equation (34). These equations can be further utilized to obtain control of continuous rotations. This could be used to generate propulsion using a rigid helical tail [22].

First, to generate propulsion in a desired direction, the robot should orient its helical tail in that direction. Once the microrobot has reached its desired rotation, a time-varying reference $\mathbf{r}(t)$ is fed through the system. Assuming that the first axis is aligned with the long axis of the helix, the propulsion reference is

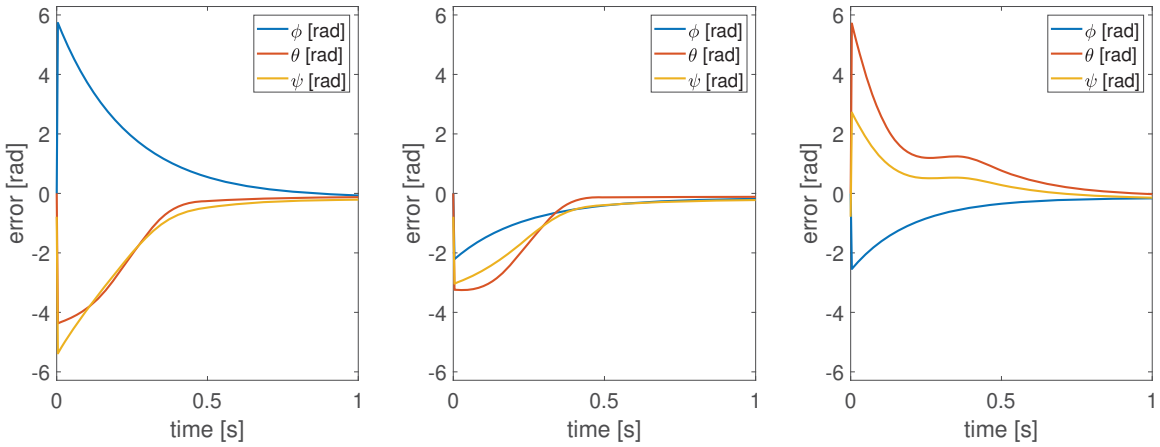

Fig. 6: Error of the position based on the three starting points described in Fig. 5. Based on the initial conditions, the time of reaching the desired position is variable, but all within the timeframe of 1 second.

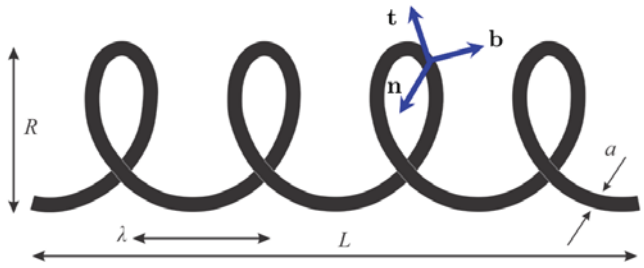

Fig. 7: Schematic representation of a helix tail used to generate propulsion by a rotational motion. This tail can be integrated to the miniature robot to provide thrust under rigid body rotation abouth the long axis of the helix

defined by

$$\begin{aligned}\mathbf{r}(t) &= -\mathbf{K}(\mathbf{\Theta}_{des} + \Delta\mathbf{\Theta}_{prop}) \\ &= \begin{bmatrix} -K_1 & 0 & 0 \\ 0 & -K_2 & 0 \\ 0 & 0 & -K_3 \end{bmatrix} \begin{bmatrix} \Theta_{des,1} + \Delta\Theta_{prop,1} \\ \Theta_{des,2} \\ \Theta_{des,3} \end{bmatrix},\end{aligned} \tag{36}$$

where $\Delta\Theta_{prop}$ is the varying propulsion angle looping on the interval $[0, 2\pi]$. When $\Delta\Theta_{prop}$ is set to increase with a constant value, the angular velocity will be constant in a discrete system. Path-mapping allows for the angular velocity to be set to a desired value. Consequently, angular velocity control allows for control of the velocity of the robot when a helical tail is used. First described by E.M. Purcell [23], a helix, shown in Figure 7, utilizes Stokes' Law to generate propulsion. Modelled after *E. coli* bacteria and their flagella bundle, the design can be utilized to generate propulsion at a low power level. The helix tail does have a low efficiency, but in the low Reynolds number environment the consumed power per unit mass propelled is lower than traditional transportation methods [24].

When applied to capsule endoscopy, a helical tail can be used to generate propulsion in a desired direction. Therefore, positional control of the capsule can be achieved using a static magnetic field. However, propulsion and orientation should be viewed as different operations. In order to change direction during propulsion, the microrobot should stop and orientate itself along the desired direction after which propulsion can resume.

2.8 Discussion of Results

The results describe a controllable system by using full state feedback. These results are gathered using simulations only, and to further study their feasibility, an actual prototype should be built and tested with.

While creating the model used to obtain the results, various assumptions were made in order to maintain consistency. The first major assumption is that the robot operates in a low Reynolds number environment, where $Re << 10$. This assumption allows for the application of Stokes' Law and the assumption that the magnetic and drag torque are equal, as is given in equation (8). Furthermore, the drag forces are not taken into account, and only the rotation of the robot is modelled. Finally, the magnetic field $\mathbf{B}$ is assumed to be uniform and constant at every position within the field. It ensures that no magnetic force is generated and the capsule achieves pure rotation.

3 CONCLUSIONS

Controllability of a microrobot embedded with an electromagnetic tri-axial coil is achieved under a full state feedback control system and demonstrated in three-dimensional space. It allows the robot to be oriented in any desired direction under the influence of a uni-directional static magnetic field. Consequently, adding a path-mapped reference to the controller allows the robot to continuously rotate around any arbitrary axis, thereby generating forward thrust force using a helical body attached to the microrobot. In conclusion, directional control of a miniature robot in a uni-directional static magnetic field is possible.

4 FUTURE WORK

To validate the results of the simulations, a prototype of a miniature robot with a tri-axial coil system and microcontroller will be designed an developed. This prototype must have the capability to measure the uni-directional static magnetic field and determine the orientation of its local frame of reference with respect to the magnetic field. Therefore, the measured states can be defined and used as an input to the system. In addition, the control system will be modified to adapt its gains in order to improve the performance and stability of the system.

REFERENCES

1. G. Iddan, G. Meron, A. Glukhovsky, and P. Swain, "Wireless capsule endoscopy," *Nature*, vol. 405, pp. 417–418, 5 2000.
2. G. Ciuti, R. Caliò, D. Camboni, L. Neri, F. Bianchi, A. Arezzo, A. Koulaouzidis, S. Schostek, D. Stoyanov, C. M. Oddo, B. Magnani, A. Menciassi, M. Morino, M. O. Schurr, and P. Dario, "Frontiers of robotic endoscopic capsules: a review," *Journal of Micro-Bio Robotics*, vol. 11, 6 2016.
3. M. Delvaux and G. Gay, "Capsule endoscopy: Technique and indications," *Best Practice and Research: Clinical Gastroenterology*, vol. 22, pp. 813–837, 10 2008.
4. A. Wang, S. Banerjee, B. A. Barth, Y. M. Bhat, S. Chauhan, K. T. Gottlieb, V. Konda, J. T. Maple, F. Murad, P. R. Pfau, D. K. Pleskow, U. D. Siddiqui, J. L. Tokar, and S. A. Rodriguez, "Wireless capsule endoscopy," *Gastrointestinal Endoscopy*, vol. 78, pp. 805–815, 12 2013.
5. C. V. d. Bruaene, "Small bowel capsule endoscopy: Where are we after almost 15 years of use?," *World Journal of Gastrointestinal Endoscopy*, vol. 7, no. 1, p. 13, 2015.
6. D. Cave, P. Legnani, R. de Franchis, and B. S. Lewis, "ICCE consensus for capsule retention," 10 2005.
7. D. A. Parikh, J. A. Parikh, G. C. Albers, and C. F. Chandler, "Acute small bowel perforation after wireless capsule endoscopy in a patient with Crohn's disease: A case report," *Cases Journal*, vol. 2, pp. 1–3, 7 2009.
8. J. S. Palmer, K. Marenah, F. El Madani, K. Jain, and S. Gupta, "Small bowel perforation following capsule endoscopy: A case report," *Annals of the Royal College of Surgeons of England*, vol. 93, p. e69, 9 2011.
9. M. K. Goenka, S. Majumder, and U. Goenka, "Capsule endoscopy: Present status and future expectation," *World J Gastroenterol*, vol. 20, no. 29, pp. 10024–10037, 2014.
10. K. B. Yesin, K. Vollmers, and B. J. Nelson, "Modeling and control of untethered biomicrorobots in a fluidic environment using electromagnetic fields," in *International Journal of Robotics Research*, vol. 25, pp. 527–536, 5 2006.
11. E. G. Quate and G. T. Gillies, "Nonlinear magnetic stereotaxis: Three-dimensional, in vivo remote magnetic manipulation of a small object in canine brain," *Medical Physics*, vol. 17, no. 3, pp. 405–415, 1990.
12. M. P. Kummer, J. J. Abbott, B. E. Kratochvil, R. Borer, A. Sengul, and B. J. Nelson, "Octomag: An electromagnetic system for 5-DOF wireless micromanipulation," *IEEE Transactions on Robotics*, vol. 26, pp. 1006–1017, 12 2010.
13. O. Erin, H. B. Gilbert, A. F. Tabak, and M. Sitti, "Elevation and Azimuth Rotational Actuation of an Untethered Millirobot by MRI Gradient Coils," *IEEE Transactions on Robotics*, vol. 35, pp. 1323–1337, 12 2019.
14. G. Shao and Y. X. Guo, "Switched Magnetic Field for Hybrid Wireless Positioning and Wireless Charging Using Helmholtz Coils," in *2019 IEEE MTT-S International Wireless Symposium, IWS 2019 - Proceedings*, Institute of Electrical and Electronics Engineers Inc., 5 2019.
15. B. J. Nelson, I. K. Kaliakatsos, and J. J. Abbott, "Microrobots for Minimally Invasive Medicine," *Annual Review of Biomedical Engineering*, vol. 12, pp. 55–85, 7 2010.
16. P. Bayly, B. Lewis, E. Ranz, R. Okamoto, R. Pless, and S. Dutcher, "Propulsive forces on the flagellum during locomotion of chlamydomonas reinhardtii," *Biophysical Journal*, vol. 100, no. 11, pp. 2716–2725, 2011.
17. I. Khalil, H. Abass, M. Shoukry, A. Klingner, R. El-Nashar, M. Serry, and S. Misra, "Robust and Optimal Control of Magnetic Microparticles inside Fluidic Channels with Time-Varying Flow Rates," *International Journal of Advanced Robotic Systems*, vol. 13, no. 3, 2016.
18. J. J. Abbott, E. Diller, and A. J. Petruska, "Magnetic Methods in Robotics," *Annual Review of Control, Robotics, and Autonomous Systems*, vol. 3, pp. 57–90, 5 2020.
19. J. Diebel, "Representing Attitude: Euler Angles, Unit Quaternions, and Rotation Vectors," tech. rep., 2006.
20. I. Khalil, L. Abelmann, and S. Misra, "Magnetic-based motion control of paramagnetic microparticles with disturbance compensation," *IEEE Transactions on Magnetics*, vol. 50, no. 10, 2014.
21. W. Ledermann, "A NOTE ON SKEW-SYMMETRIC DETERMINANTS," tech. rep., 1991.
22. T. Xu, J. Yu, X. Yan, H. Choi, and L. Zhang, "Magnetic Actuation Based Motion Control for Microrobots: An Overview," *Micromachines*, vol. 6, pp. 1346–1364, 9 2015.
23. E. M. Purcell, "Life at low Reynolds number," *American Journal of Physics*, vol. 45, pp. 3–11, 1 1977.

24. E. M. Purcell, “The efficiency of propulsion by a rotating flagellum,” *Proceedings of the National Academy of Sciences of the United States of America*, vol. 94, pp. 11307–11311, 10 1997.